Structures and Surface Energies of (100) and Octopolar (111) Faces of Halite (NaCl): an Ab initio Quantum−Mechanical and Thermodynamical Study

ARTICLE *in* CRYSTAL GROWTH & DESIGN · JULY 2008

Impact Factor: 4.89 · DOI: 10.1021/cg8000027

4 AUTHORS:

Marco Bruno
Università degli Studi di Torino
84 PUBLICATIONS **706** CITATIONS
SEE PROFILE

Dino Aquilano
Università degli Studi di Torino
190 PUBLICATIONS **998** CITATIONS
SEE PROFILE

Linda Pastero
Università degli Studi di Torino
71 PUBLICATIONS **350** CITATIONS
SEE PROFILE

Mauro Prencipe
Università degli Studi di Torino
74 PUBLICATIONS **1,122** CITATIONS
SEE PROFILE

CRYSTAL GROWTH & DESIGN
2008
VOL. 8, NO. 7
2163–2170

Structures and Surface Energies of (100) and Octopolar (111) Faces of Halite (NaCl): an Ab initio Quantum-Mechanical and Thermodynamical Study

Marco Bruno,* Dino Aquilano, Linda Pastero, and Mauro Prencipe

Dipartimento di Scienze Mineralogiche e Petrologiche, Università degli Studi di Torino, Via Valperga Caluso 35, I-10125 Torino, Italy

Received January 2, 2008; Revised Manuscript Received February 19, 2008

ABSTRACT: The structures of the (100), octopolar (111) Na-terminated [$(111)^{Na}$], and (111) Cl-terminated [$(111)^{Cl}$] surfaces of halite (NaCl) were determined by means of ab initio quantum mechanical calculations (density functional theory, DFT). The (111) surfaces show higher surface relaxation with respect to the (100) surface. The surface energies (γ) at $T = 0$ K for relaxed and unrelaxed (100) and (111) faces were determined at DFT level. The values of the surface energy for the relaxed faces are $\gamma_{(100)} = 160$, $\gamma_{(111)^{Cl}} = 390$ and $\gamma_{(111)^{Na}} = 405$ erg/cm^2; therefore, the stability order of relaxed surfaces reads: (100) < $(111)^{Cl}$ < $(111)^{Na}$. For the unrelaxed faces, the surface energies are higher: $\gamma_{(100)} = 161$, $\gamma_{(111)^{Cl}} = 552$ and $\gamma_{(111)^{Na}} = 551$ erg/cm^2.To check if the octopolar (111) faces can belong to the equilibrium morphology of the crystal/vapor system, the relaxed surface energies at $T > 0$ K were calculated by considering both the vibrational motion of atoms and the surface configurational entropy. From these calculations it resulted that the octopolar $(111)^{Na}$ and $(111)^{Cl}$ faces cannot belong to the equilibrium morphology. Octopolar reconstruction and both surface vibrational and configurational entropy then allow us to explain why the {111} NaCl form cannot enter the equilibrium shape of the crystal.

Introduction

The halite (NaCl) crystal is cubic with space group *Fm*3*m* and $Z = 4$ (four formula units per cell); the lattice parameter is $a = 5.6401(2)$ Å at room temperature, as determined by X-ray diffraction measurements by Walker et al.[1] on synthetic NaCl powders.

The NaCl crystals obtained from vapor growth show exclusively the {100} form at temperatures below $T_0 \approx 920$ K.[2,3] Above T_0, rounded regions having centers with {111} orientations appear at the cube corners and grow as the temperature is increased. At ~1000 K, these rounded regions coalesce, so that neither sharp edges nor faceting between the {100} faces remain.

The morphology of NaCl crystals grown from aqueous solution results to be richer. In fact, in that case they show {110} and {111} forms when a given amount of specific impurity (e.g., urea, formamide, $CdCl_2$) is added to the growth medium.[4,5] Some works reported that {111} NaCl faces can also be obtained from pure water solution.[4,6] It was observed that if NaCl like crystals grow at high supersaturation, well-developed {111} faces appear. On the other hand, if they were grown at low supersaturation, only cubic crystals were formed.

In the past, particular attention had been paid to the study of the polar {111} faces of crystals with rocksalt-type structure, which are expected to be not stable. Along the ⟨111⟩ directions, the crystals with NaCl structure consist of alternating layers of cations and anions (Figure 1a). Therefore, the (111) surface must have an highly divergent electrostatic energy, which makes this surface theoretically unstable and not present in the equilibrium morphology of NaCl-type crystals. To explain the presence of the {111} form in ionic crystals with rocksalt-type structures grown from aqueous solution, researchers then invoked the adsorption of impurities, H_2O molecules, and/or H^+ and OH^- ions.[7,8] Instead, when no impurities are present, theoretical calculation suggests two possibilities to stabilize the {111} surfaces: (a) the bulk terminated {111} surfaces break up into neutral {100} facets upon annealing[8] or (b) the surfaces reconstruct. The latter hypothesis was originally suggested by Lacmann,[9] who postulated that all the NaCl surfaces should be reconstructed in such a way that the finite crystal only terminates with complete $(NaCl)_4$ molecules (octopoles). Accordingly, the outermost layer of the (111) surface contains only 1/4 of the available lattice sites, whereas the two layers below contain 3/4 and 4/4 of the sites, respectively (Figure 1b): in the case of the NaCl crystals the octopolar {111} surfaces may be either Na or Cl terminated; in what follows, the first one will be indicated by $(111)^{Na}$, and the other one by $(111)^{Cl}$.

This way of reconstructing shows two main advantages: first, the {111} octopolar reconstructed surfaces are the only ones that respect the symmetry of the surface point group; second, it provides a simple thermodynamical ground state that does not require point defects or kinetic phenomena (such as adsorption of impurities during growth) for its stabilization. Wolf[10] confirmed this "octopole" reconstruction hypothesis, which cancels the divergence of the electric field at the {111} crystal surfaces, by calculations of the (111) NaCl surface energy in contact with vacuum. Furthermore, the octopolar structure has been confirmed for the (111) surface of NiO.[11] Nevertheless, reconstructed octopolar {111} surfaces were never observed in NaCl crystals, neither at equilibrium nor during growth from the vapor phase.

In this paper, we aim at considering, for the first time, all the factors that can contribute to determine the more realistic value of the {111} surface energy (at the temperature of the experiments done till now) for the crystal/vapor interface. This is a necessary but not sufficient stage to be reached before evaluating the contribution due to the water adsorption, in order to determine the (111) surface energy at the crystal/solution interface. Our reasoning is supported by the recent results we obtained when calculating the equilibrium shape of calcite crystal through the surface energy values of the crystal/solution interfaces.[12] As a matter of fact, we found that only by

* Corresponding author. E-mail: marco.bruno@unito.it. Tel.: 390116705131. Fax: 390116705128.

10.1021/cg8000027 CCC: $40.75
Published on Web 06/17/2008

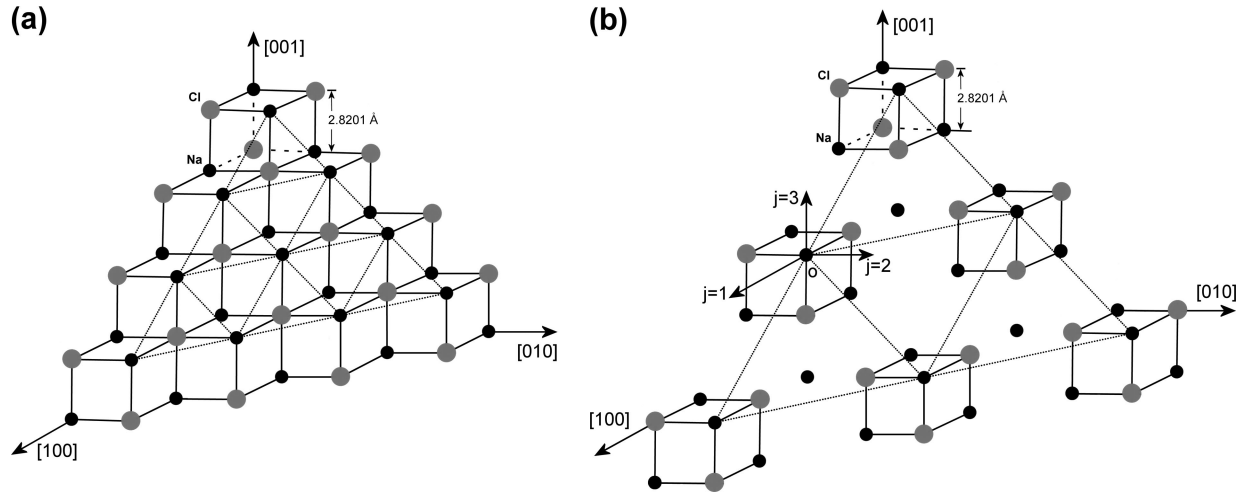

Figure 1. Unrestructured (a) and restructured (b) (111) Na-terminated surfaces of NaCl are drawn. The restructured $(111)^{Na}$ face is made up by $(NaCl)_4$ molecules (octopoles): the outermost layer of the $(111)^{Na}$ surface contains only 1/4 of the available lattice sites, whereas the two layers below contain 3/4 and 4/4 of the sites, respectively. The dotted line joins the atoms belonging to the outermost layer.

considering all the factors determining the surface energy values it is possible to explain the old discrepancies found in literature between experimental and theoretical findings. Thus, we obtained detailed information on the structure of the (100), $(111)^{Na}$ and $(111)^{Cl}$ surfaces of NaCl crystals. We performed a quantum mechanical study of the bulk and (100), $(111)^{Na}$ and $(111)^{Cl}$ surfaces structure, whose geometries were optimized at DFT (density functional theory) level. Furthermore, to verify if the octopolar (111) face can belong to the equilibrium morphology of halite grown from vapor, the surface energies at $T \geq 0$ K of the (100), $(111)^{Na}$, and $(111)^{Cl}$ faces were determined and their relative stability evaluated. The surface energy at $T > 0$ K was calculated by taking into account both the vibrational motion of atoms (vibrational entropy) in the bulk and at its surface, and the surface configurational entropy. For this purpose, a previous thermodynamical model[13] developed for unrestructured surfaces, was extended and applied to the restructured ones.

Computational Details

Bulk and slab geometry optimizations were performed by means of the ab initio CRYSTAL06 code,[14] which implements the Hartree−Fock and Kohn−Sham, self-consistent field (SCF) method for the study of periodic systems.[15]

Hamiltonian and Computational Parameters. The calculations were performed at DFT level. The B3LYP Hamiltonian[16] has been used, which contains a hybrid Hartree−Fock/density functional exchange-correlation term. The exchange-correlation contribution is evaluated numerically by integrating, over the cell volume, a function of the electron density and of its gradient. The choice of the grid of points for the integration is based on an atomic partition method, originally developed by Becke.[17] In the present case, the default pruned (55, 434) p grid was chosen, which ensures a satisfactory accuracy in geometry optimization.[14]

The thresholds (ITOL1, ITOL2, ITOL3, ITOL4, and ITOL5) controlling the accuracy of the calculation of Coulomb and exchange integrals[14] were set to 1×10^{-7} (ITOL1 to ITOL4) and 1×10^{-14} (ITOL5). The diagonalization of the Hamiltonian was performed at 10 **k** points in the reciprocal space (Monkhrost net[18]) by setting the shrinking factor IS[14] to 8. To check the convergence of the results with respect to the computational parameters, bulk geometry optimization was repeated by setting ITOL1−ITOL4 to 1×10^{-8} and ITOL5 to 1×10^{-16}, and no significant differences have been observed.

Geometry optimization is considered converged when each of the components of the gradient and of the displacement (TOLDEG, TOLDEX parameters in CRYSTAL06) are smaller than 0.0003 hartree bohr^{-1} and 0.0012 bohr, respectively.

Table 1. Cell Parameter, *a*, and Na−Cl Distance (Å) Calculated at the DFT level (B3LYP)

	B3LYP	HF	exp
a	5, 7373	5, 80	5, 6401
Na−Cl	2, 8687	2, 90	2, 8201

The experimental (exp[1]) and Hartree−Fock (HF[23]) values are reported for comparison.

Basis Set. The multielectronic wave function is constructed as an antisymmetrized product (Slater determinant) of monoelectronic crystalline orbitals (CO), which are linear combinations of local functions (to be indicated as AO's) centered on each atom of the crystal. In turn, AO's (basis set) are linear combinations of Gaussian-type functions (GTF, the product of a Gaussian times a real solid spherical harmonic to give s- and p-type AO's). In the present case, Na is described with a 8−511G basis.[19] It consists of eight contracted GTF's for the description of the s shell, five contracted GTF's for the description of the sp inner shell, and two uncontracted functions for the valence sp shells. For Cl, the basis sets 86−311G[20] was used. The variationally reoptimized exponent of the uncontracted shells are 0.348 (sp) for Na, and 0.298 (sp) and 0.107 bohr^{-2} (sp) for Cl.

Geometry Optimization. The bulk geometry (lattice parameter) was optimized at DFT level, starting from the experimental value[1] determined by X-ray powder diffraction data at room temperature (Table 1).

Geometry optimizations (lattice parameters and fractional coordinates) of (100) and (111) slabs have been done with thickness up to 20 and 9 layers, respectively; lattice parameters and atomic coordinates of the 20-layer (100) and 9-layer (111) slabs are listed in Tables SI−SIII in the Supporting Information. However, we have ascertained that the considered thickness are sufficient to reproduce bulklike properties at the center of the slabs and to obtain an accurate description of the surfaces. Each slab of given thickness was generated by cutting the experimental bulk structure parallel to the face of interest [(100), $(111)^{Na}$, and $(111)^{Cl}$], and eliminating the atoms in excess in the case of the (111) face, in order to perform the octopolar reconstruction. All of the slab optimizations were done at B3LYP level.

The optimization of lattice parameters and atomic coordinates, both in the bulk and in the slab, was performed by means of a modified conjugate gradient algorithm[21] as implemented in CRYSTAL06.[14]

Calculation of the Surface Energy at 0 K. The surface energy at 0 K [$\gamma(0)$] has been calculated by means of the following relation[22]

$$\gamma(0) = \lim_{n\to\infty} E_s(n) = \lim_{n\to\infty} \frac{E(n) - n[E(n) - E(n-1)]}{2A} \qquad (1)$$

where A is the area of the primitive unit cell of the surface, and $E(n)$ is the energy of a n-layer slab; the factor 2 in the denominator accounts

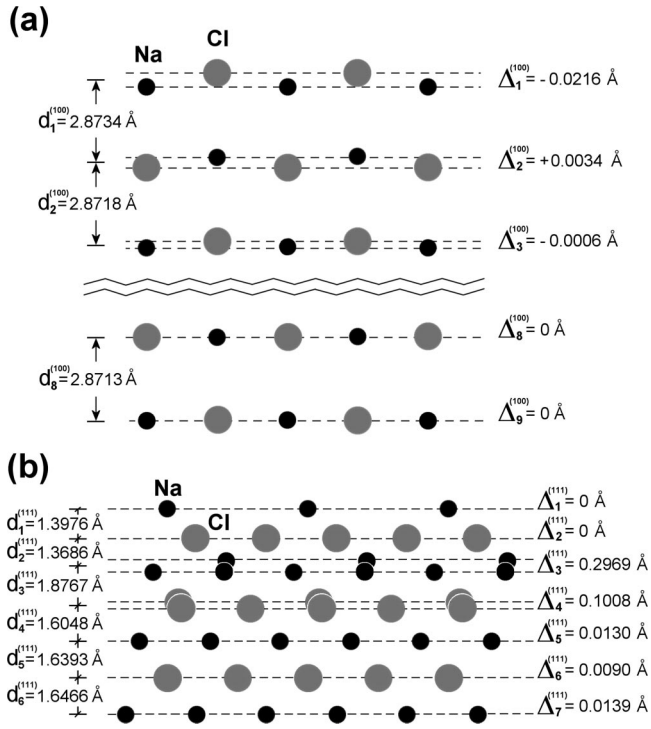

Figure 2. Schematic representations of the relaxed structures (a) of the (100) slab viewed along the [100] direction and (b) of the octopolar $(111)^{Na}$ slab viewed along a direction perpendicular to [111].

for the upper and lower surfaces of the slab. $E_s(n)$ is thus the energy per unit area required to form the surface from the bulk. As more layers are added in the calculation ($n \rightarrow \infty$), $E_s(n)$ will converge to the surface energy per unit area, $\gamma(0)$. The surface energy has been calculated at DFT level, for the (100), $(111)^{Na}$, and $(111)^{Cl}$ faces.

Results and Discussion

Bulk Structure. Table 1 lists the cell parameter (a) and the Na−Cl distance calculated in the bulk optimization. The difference between calculated and experimental cell parameter results to be ∼1.6%. In Table 1 is also reported the cell parameter determined at Hartree−Fock level,[23] which is higher by ∼ 1.2% than the value calculated at DFT level; such results are consistent with what is generally observed concerning the influence of the Hamiltonian on cell parameters; see for example Dovesi et al.[22] for a discussion on NaCl.

(100) Surface Structure. The (100) face of halite, observed along the [100] direction, consists of electrically neutral layers. In Figure 2a, the optimized (100) surface is reported. To describe the (100) slab structure, we use the following parameters[24]

$$\Delta_i^{(100)} = \frac{1}{2}\left(x_i^{Na} - x_i^{Cl}\right) \quad (2)$$

$$d_i^{(100)} = \frac{1}{2}\left(x_{i+1}^{Na} + x_{i+1}^{Cl} - x_i^{Na} - x_i^{Cl}\right) \quad (3)$$

where x_i^{Na} and x_i^{Cl} are the absolute coordinates along [100] of Na and Cl, respectively, in the i-th layer (for $i = 1,..., n$). $\Delta_i^{(100)}$ is the average rumpling of the i-th layer; it corresponds to the vertical dislocations of equal magnitude, but opposite sign of the cations and anions out of the geometrical average of the layer. A positive rumpling is connected to an outward movement of the cations, a negative one to an inward motion. $d_i^{(100)}$ is the average distance to the next underlying layer. In Figure 3a, the values of these parameters as a function of layer i of the slab are reported.

A slight deviation in the optimized geometry of the (100) slab from the ideal bulk geometry is observed. In the first layer, the Na cations are shifted inward and Cl anions are shifted outward, $\Delta_1^{(100)} = -0.0216$ Å, but in the underneath layers, $\Delta_i^{(100)}$ converges rapidly to zero: $\Delta_i^{(100)}$ is 0.0034, −0.0006, and 0 Å in the second, third, and fourth layers, respectively. The structural parameter $\Delta_i^{(100)}$ calculated in the present study is in good agreement with that obtained in the experimental observations,[24−26] $\Delta_1^{(100)}$=−0.06(3)−0.07(3), $\Delta_2^{(100)}$=0.00(3)−0.01(4), and $\Delta_3^{(100)}$ = 0.00(3) Å.

We did not observe significant differences between the $d_i^{(100)}$ distances throughout the slab: $d_1^{(100)}$ = 2.8734 Å is higher by ∼0.06 and ∼0.16% with respect to $d_2^{(100)}$ and the optimized bulk value (2.8687 Å; Table 1), respectively. These values are larger than the experimental ones,[24,26] $d_1^{(100)}$ = 2.76(3)−2.78(3), $d_2^{(100)}$ = 2.77(3)−2.80(3), and $d_3^{(100)}$ = 2.81(5) Å. The differences between experimental and calculated distances are in line with those observed for the cell parameter a, because the B3LYP Hamiltonian tends to overestimate these structural parameters.

$(111)^{Na}$ and $(111)^{Cl}$ Surface Structures. The (111) face of halite, observed along a direction perpendicular to [111], is

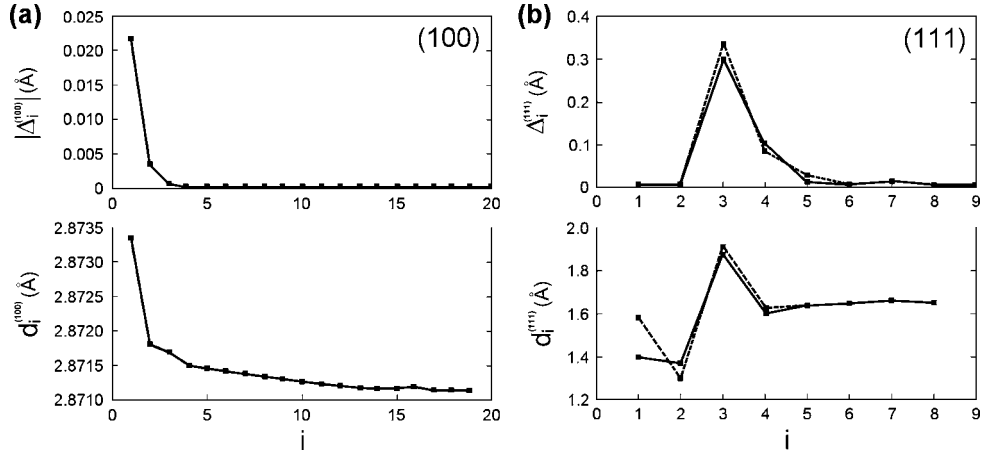

Figure 3. (a) Rumpling, $\Delta_i^{(100)}$, and the average interlayer distances, $d_i^{(100)}$, in the (100) slab. (b) Rumpling, $\Delta_i^{(111)}$, and the average interlayer distances, $d_i^{(111)}$, in the (111) slab. The parameters are reported as a function of the layer $i = 1,..., n$; solid line, $(111)^{Na}$ slab; dotted line $(111)^{Cl}$ slab. See text for details.

Table 2. Surface Energies of the Relaxed, γ^r, and Unrelaxed, γ^u, (100), $(111)^{Na}$, and $(111)^{Cl}$ Faces

	γ^r		γ^u	
	erg/cm^2	kcal/(mol Å^2)	erg/cm^2	kcal/(mol Å^2)
(100)	160	0.230288	161	0.231727
$(111)^{Na}$	405	0.582917	551	0.793054
$(111)^{Cl}$	390	0.561327	552	0.794494

composed by alternating layers of Na and Cl ions; in Figure 2b, the optimized $(111)^{Na}$ surface is reported. To describe the (111) slab structure we use the following parameters

$$\Delta_i^{(111)} = \frac{1}{2}\left(x_i^h - x_i^l\right) \quad (4)$$

$$d_i^{(111)} = \frac{1}{2}\left(x_{i+1}^h + x_{i+1}^l - x_i^h - x_i^l\right) \quad (5)$$

The meaning of such parameters is the same of those in eqs 2 and 3, but they are calculated by considering the absolute coordinates of the ions along [111] in the *i*-th layer; h and l indicate the highest and lowest ion (Na or Cl) in the *i*-th layer. In Figure 3b, the values of these parameters for the $(111)^{Na}$ and $(111)^{Cl}$ slabs are reported.

With reference to the $\Delta_i^{(111)}$ parameter, no significant differences exist between the $(111)^{Na}$ and $(111)^{Cl}$ slabs; in both cases, $\Delta_1^{(111)} = \Delta_2^{(111)} = 0$ by symmetry and the rumpling only involves the layers $i = 3, 4, 5$ (see Figure 3b). Instead, a larger difference is noted in the layer distance $d_1^{(111)}$, which is ~1.40 Å in the $(111)^{Na}$ slab and ~1.60 Å in the $(111)^{Cl}$ slab.

Surface Energies of (100), $(111)^{Na}$, and $(111)^{Cl}$ Faces. The resulting values of the relaxed surface energies (γ^r) are reported in Table 2; the stability order of the relaxed surfaces is (100) $\ll$ $(111)^{Cl}$ < $(111)^{Na}$.

The surface energies for the unrelaxed faces (γ^u) have also been determined (Table 2). The calculations have been carried out by considering an increasing number of layers cut from the bulk equilibrium geometry obtained at DFT level (Table 1). As expected, the latter turned out to be greater than those obtained for the relaxed faces. Furthermore, the unrelaxed surface energies of the $(111)^{Cl}$ and $(111)^{Na}$ faces are equal; therefore the relative stability order of the unrelaxed surfaces is (100) $\ll$ $(111)^{Cl} = (111)^{Na}$.

In the past, different estimates of the $\gamma_{(100)}$ have been obtained. Experimental surface energy measurements of NaCl have led to a large range of values, 180−380 erg/cm^2; see Li et al.[27] for detailed information on these works. A wide range of values (at 0 K) was also determined in theoretical works. In particular, Shi and Wortis,[3] by using empirical potentials (Born−Mayer−Huggins, BMH,[28] and Catlow−Diller−Norget, CDN,[29] potentials), obtained $\gamma^r_{(100)}$= 124−212 and $\gamma^u_{(100)}$= 186−224 erg/cm^2. The CDN potential was also used by Wolf,[10] who calculated very similar surface energies for the relaxed and unrelaxed (100) faces, $\gamma^r_{(100)} = 223$ and $\gamma^u_{(100)} = 225$ erg/cm^2, respectively. In a recent work, Li et al.[27] performed DFT calculations (LDA,[30] PBE GGA,[31] and PBE-WC,[32] functionals) on the (100) slab of NaCl, obtaining $\gamma^r_{(100)} = 234$ (LDA), 144 (PBE GGA), and 151 (PBE-WC) erg/cm^2. Our estimate of $\gamma^r_{(100)}$ results in good agreement with those obtained by Li et al.[27] with the PBE GGA and PBE-WC functionals.

In the case of the (111) face, the only values of the surface energy at 0 K are given by Wolf,[10] $\gamma^r_{(111)} = 541$ (CDN potential) and $\gamma^u_{(111)} = 693$ erg/cm^2, and Shi and Wortis,[3] $\gamma^u_{(111)} = 659$ (BMH) to 684 (CDN) erg/cm^2. They considered an octopolar reconstruction of the (111) surface and obtained the same surface energy value for the $(111)^{Na}$ and $(111)^{Cl}$ faces. According to our calculations this is true for the unrelaxed $(111)^{Na}$ and $(111)^{Cl}$ surfaces, whereas a difference of 15 erg/cm^2 is observed between the relaxed ones (Table 2). In addition, we obtain both the relaxed and unrelaxed $\gamma_{(111)}$ values, which are noteworthily lower than the surface energies estimated by Wolf[10] and Shi and Wortis.[3]

The surface energy is a basic thermodynamical quantity, of crucial importance to determine the equilibrium shape of crystals. Up to now, we have considered the surface energy at $T = 0$ K, but it is fundamental to know how this quantity changes with temperature ($T > 0$ K). A simple temperature effect we have to consider is that due to the vibrational motion of atoms in the crystal and at its surface. To analyze this aspect we adapted a model proposed by Kern,[13] which is based on a monatomic Einstein crystal, where each atom coincides with a three-dimensional harmonic oscillator whose motion is supposed to be not coupled to that of the other atoms (for the derivation of the model, see appendix A). The relation valid at high temperatures resulting from this treatment is the following

$$\gamma_\sigma(T) = \gamma_\sigma(0) + \frac{k_B\theta}{2}\sum_{k=1}^{p}\left\{n_{k,\sigma}\sum_{j=1}^{3}\left[\left(\frac{\sum_{l=1}^{m_{k,\sigma}}(\cos\varphi_{k,l,j,\sigma})^2}{\sum_{l=1}^{m_b}(\cos\varphi_{l,j,b})^2}\right)^{\frac{1}{2}} - 1\right]\right\} + k_B T\sum_{k=1}^{p}\left[n_{k,\sigma}\ln\prod_{j=1}^{3}\left(\frac{\sum_{l=1}^{m_{k,\sigma}}(\cos\varphi_{k,l,j,\sigma})^2}{\sum_{l=1}^{m_b}(\cos\varphi_{l,j,b})^2}\right)^{\frac{1}{2}}\right] \quad (6)$$

where $\gamma_\sigma(T)$ is the surface energy of the face σ [(100), $(111)^{Na}$, or $(111)^{Cl}$] at temperature T; $\gamma_\sigma(0)$ is the surface energy at 0 K (Table 2); $j = 1, 2, 3$ are three orthogonal axes lying along the 4-fold symmetry axes of the crystal ([100] $\equiv j = 1$; [010] $\equiv j$

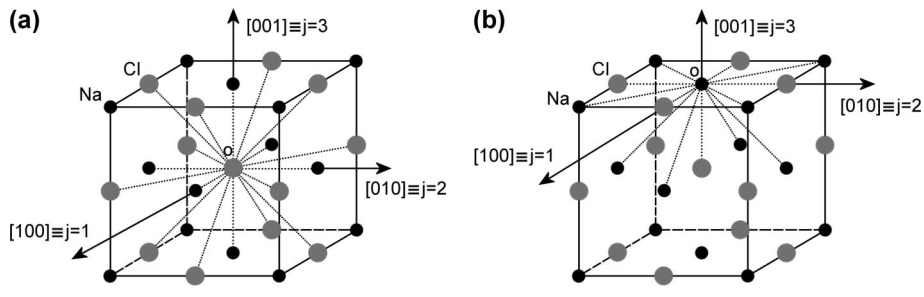

Figure 4. First nearest-neighbor atom polyhedron centered on the atom O in (a) the bulk crystal and (b) the (100) surface of NaCl. See text for details.

$= 2$; [001] $\equiv j = 3$; Figure 4); $p = 1$ for the (100) face (Figure 4b), where every surface atom is coordinated by the same number of first neighbors ($m_{1,(100)} = 13$); $p = 3$ for the restructured (111) surface (Figure 1b); its outermost layer ($k = 1$) contains only 25% of the available lattice sites with a coordination polyhedron formed by six atoms ($m_{1,(111)} = 6$), the two layers below contain 75% ($k = 2$) and 100% ($k = 3$) of the sites, with $m_{2,(111)} = 11$ and $m_{3,(111)} = 15$, respectively (for an atom in the NaCl bulk, $m_b = 18$; Figure 4a); $n_{k,\sigma}$ is the surface atomic density (atoms cm^{-2}) in the k-th layer of the surface σ; $\varphi_{k,l,j,\sigma}$ is the angle formed by the axis j and a vector $A_{k,l,\sigma} - O_{k,\sigma}$ joining an atom $O_{k,\sigma}$ in the k-th layer of the surface σ to an atom $A_{k,l,\sigma}$ of the first neighbor polyhedron centered on $O_{k,\sigma}$; $\varphi_{l,j,b}$ is the angle formed by the axis j and a vector joining an atom O_b in the bulk and an atom $A_{l,b}$ of the first neighbor polyhedron centered on O_b; k_B is the Boltzmann's constant; θ is the Debye temperature of the solid ($\theta = 321$ K, for NaCl[33]).

By considering unrelaxed surfaces (Figures 1b and 4b), for the sake of simplicity, we calculated the following quantities to insert in eq 6

$$\sum_{l=1}^{m_b}(\cos\varphi_{l,1,b})^2 = \sum_{l=1}^{m_b}(\cos\varphi_{l,2,b})^2 = \sum_{l=1}^{m_b}(\cos\varphi_{l,3,b})^2 = 6$$

$$\sum_{l=1}^{m_{1,(100)}}(\cos\varphi_{1,l,1,(100)})^2 = \sum_{l=1}^{m_{1,(100)}}(\cos\varphi_{1,l,2,(100)})^2$$

$$= 5 \neq \sum_{l=1}^{m_{1,(100)}}(\cos\varphi_{1,l,3,(100)})^2 = 3$$

$$\sum_{l=1}^{m_{1,(111)}}(\cos\varphi_{1,l,1,(111)})^2 = \sum_{l=1}^{m_{1,(111)}}(\cos\varphi_{1,l,2,(111)})^2 =$$

$$\sum_{l=1}^{m_{1,(111)}}(\cos\varphi_{1,l,3,(111)})^2 = 2$$

$$\sum_{l=1}^{m_{2,(111)}}(\cos\varphi_{2,l,1,(111)})^2 = 5 \neq \sum_{l=1}^{m_{2,(111)}}(\cos\varphi_{2,l,2,(111)})^2 =$$

$$\sum_{l=1}^{m_{2,(111)}}(\cos\varphi_{2,l,3,(111)})^2 = 3$$

$$\sum_{l=1}^{m_{3,(111)}}(\cos\varphi_{3,l,1,(111)})^2 = \sum_{l=1}^{m_{3,(111)}}(\cos\varphi_{3,l,2,(111)})^2 =$$

$$\sum_{l=1}^{m_{3,(111)}}(\cos\varphi_{3,l,3,(111)})^2 = 5 \quad (7)$$

Then, using the surface densities (number of atoms/cm^2) $n_{1,(100)} = 1.26 \times 10^{15}$, $n_{1,(111)} = 1.815 \times 10^{14}$, $n_{2,(111)} = 5.446 \times 10^{14}$, $n_{3,(111)} = 7.261 \times 10^{14}$, and the relaxed surface energy values at 0 K reported in Table 2, we calculated the surface energy at $T > 0$ K of the (100), (111)^{Na}, and (111)^{Cl} faces (Figure 5). We observe a decrease of $\sim$110 erg/cm^2 for the $\gamma^r_{(100)}$ in the temperature range 0−1070 K ($T_m = 1070$ K, melting temperature of NaCl[34]), being $(d\gamma/dT)_{(100)} = -0.092$ erg/(cm^2 K). This value is in excellent agreement with that calculated by Zykova-Timan et al.[35] by means of molecular dynamics simulation with Born-Mayer-Huggins-Fumi-Tosi (BMHFT[36]) two-body potential, but it is considerably lower than that obtained by Mulheran,[37] $(d\gamma/dT)_{(100)} = -0.06$ erg/(cm^2 K), by considering a not specified empirical potential and the correlation between the ionic vibrations.

In the same temperature range, a higher decrease ($\sim$150 erg/cm^2) of $\gamma^r_{(111)^{Na}}$ and $\gamma^r_{(111)^{Cl}}$ is observed, being $(d\gamma/dT)_{(111)} = -0.140$ erg/(cm^2 K). The comparison of this result with those obtained in previous works is not possible because, to the best of our knowledge, the variation in the surface energy with the temperature of the octopolar (111) face was never determined.

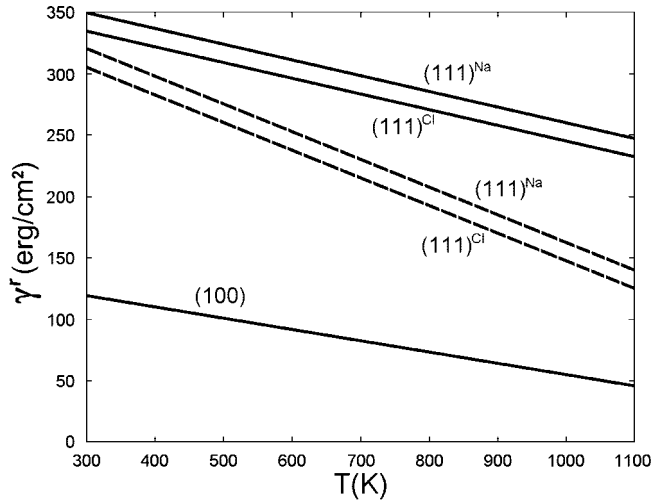

Figure 5. Surface energies of the (100), (111)^{Na}, and (111)^{Cl} faces reported as a function of temperature. Solid line, surface energies calculated without considering the configurational entropy; dashed line, surfaces energies calculated taking into account the configurational entropy.

A more accurate estimate of $\gamma_\sigma(T)$ also requires the knowledge of the configurational entropy of the crystal surface. According to Hunt and Gale[38] model, the configurational entropy of a (100) face of a monatomic fcc crystal only reduces the surface energy by $\sim$5% at the melting temperature (see also Shi and Wortis[3]). Therefore, we may neglect this contribution to the (100) surface energy, as such variation is probably lower than the error introduced in the simplified model we used to estimate the atomic vibrational effect on the energy. On the contrary, the configurational entropy is not negligible in the case of the (111) face. Shi and Wortis[3] obtained a relation that gives an approximate estimate of $E_{C(111)}$, the surface configurational energy of the (111) face of NaCl

$$E_{C(111)} = -k_B T(0.323)\frac{\sqrt{3}}{d^2} \quad (8)$$

where d is the interionic distance (2.8102 Å). By adding eq 8 to eq 6, we calculated again $\gamma^r_{(111)^{Na}}$ and $\gamma^r_{(111)^{Cl}}$ (Figure 5). In the temperature range 0−1070 K, the configurational term causes a further decrease of $\sim$100 erg/cm^2 in the surface energy of the (111)^{Na} and (111)^{Cl} faces. On the whole, by taking into account both the vibrational motion of the atoms and the configurational energy, the surface energy of the (111)^{Na} and (111)^{Cl} faces decrease of $\sim$250 erg/cm.[2]

By using the relation $\sqrt{3}\gamma_{(100)}(T_0) = \gamma_{(111)}(T_0)$, we determined the temperature T_0 at which the (111) face should appear in the equilibrium morphology of NaCl crystals: $T_0 = 2015$ and 1800 K for the (111)^{Na} and (111)^{Cl} surfaces, respectively. Then, according to our calculation, the octopolar (111)^{Na} and (111)^{Cl} faces cannot belong to the equilibrium morphology of a NaCl crystal grown from vapor, with T_0 being greater than T_m.

Conclusions

Bulk and (100), (111)^{Na}, and (111)^{Cl} slab optimizations of halite (NaCl) were performed at DFT level. The (111)^{Na} and (111)^{Cl} surfaces relax more than the (100) surface. The latter

shows small deviations from the bulk geometry: the Na shifted inward and Cl shifted outward with respect to the geometrical mean of the layer (Figure 2a). Furthermore, the $(111)^{Na}$ and $(111)^{Cl}$ surfaces suffer a very similar surface relaxation.

The surface energies at 0 K for relaxed and unrelaxed (100), $(111)^{Na}$ and $(111)^{Cl}$ faces, were determined at DFT level. The stability order is (100) $\ll$ $(111)^{Cl}$ < $(111)^{Na}$ for the relaxed surfaces and (100) $\ll$ $(111)^{Cl} = (111)^{Na}$ for the unrelaxed ones.

The relaxed surface energy at 0 K of the octopolar (111) faces (Table 2) results to be noteworthy lower than that calculated by Mulheran,[37] 550 erg/cm^2, for the (111) face reconstructed by removing half-ions from the top of the slab and replacing them on the bottom of the stack. Such a difference in the energy values suggests that the correct way to reconstruct the (111) surface of crystals with rocksalt-type structure is that proposed by Lacmann.[9] This is reasonable also from the point of view of the bulk crystal symmetry, which cannot be arbitrarily interrupted at the crystal surface, as previously demonstrated by Massaro et al.[12] for the (01.2) face of calcite. In fact, the only way to preserve the 3-fold axis perpendicular to the (111) surface is to consider the octopolar reconstruction, because any other reconstructed surface profile does not respect the crystal field imposed by the bulk.

The effect of temperature on relaxed surface energy was also taken into account. The surface energy at $T > 0$ K was calculated by considering the vibrational motion of atoms and the surface configurational entropy (Figure 5). Furthermore, according to our calculations the octopolar $(111)^{Na}$ and $(111)^{Cl}$ faces cannot belong to the equilibrium morphology of a NaCl crystal grown from vapor.

Even if our calculations confirms that {111} form cannot enter the equilibrium shape of NaCl crystal grown from vapor, the result we obtained allows us to foresee an ultimate answer to the following age-old and unsolved questions, namely the following:

(i) Can water adsorption allow the {111} form to enter the equilibrium shape of NaCl crystal in pure aqueous solution?[39]

(ii) Is the observed {111} form entering the shape of NaCl growing from pure aqueous solution due to a thermodynamic or kinetic effect?

In fact, it is reasonable to assume that water adsorption on the kinked (111) NaCl surface (reconstructed) should lower its surface energy value much more than that of the flat (100) NaCl surface. Hence, when considering the cooperative effect of vibrational and configurational entropies along with that of water adsorption, it is not hazardous to imagine that the relation $\gamma_{(111)} \leq \sqrt{3}\gamma_{(100)}$ should be fulfilled even at room temperature.

An analogous problem has been recently faced when analyzing the competition in the equilibrium shape of calcite crystals, between the {10.4} and {01.2} forms.[12] In this case, it was shown for the first time that at variance with the common opinion that the cleavage (10.4) rhombohedron is the only form belonging to the equilibrium crystal shape, another flat and reconstructed face, (01.2), can compete with the (10.4) one thanks to the contribution of both the entropy factors and the water adsorption, for entering the equilibrium shape.

Future works will be devoted to the development of an improved model for the calculation of the surface energy at $T > 0$ K, in which the anharmonic effects and long-range interactions are considered. At the same time, ab initio quantum-mechanical calculations of the surface vibrational entropy and water molecules/surface interaction on NaCl slabs will be performed and the results compared with those of the model.

Acknowledgment. The authors acknowledge the MUR (Ministero dell'Università e della Ricerca) for funding (PRIN 2005).

Appendix

The Kern's model[13] was developed to study how the surface energy (γ) of a monatomic Einstein crystal is modified with temperature (T), by taking into account the vibrational motion of the atoms in the crystal and at its surface. In the Kern's model the surfaces energy of the face σ is calculated with the relation:

$$\gamma_\sigma(T) = n_\sigma(F_\sigma - F_b) \tag{A1}$$

where n_σ is the surface density (number of atoms/cm^2), and F_σ and F_b are the free energies of a surface and bulk (b) atom, respectively. Equation A1 is only valid for unrestructured surfaces (Figure A1a). To take into account the surface reconstruction (Figure A1b), where the interface is not planar and different levels of atoms are exposed, we defined the surface energy in a different way

$$\gamma_\sigma(T) = \sum_{k=1}^{p} n_{k,\sigma}(F_{k,\sigma} - F_b) \tag{A2}$$

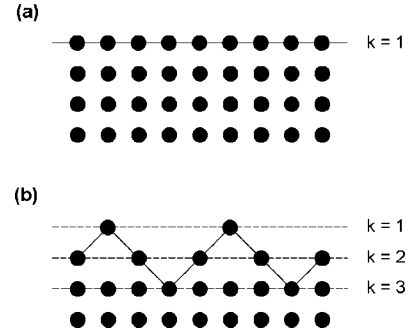

Figure A1. (a) Unrestructured and (b) restructured surfaces. In the unrestructured surface (a), only one surface layer can be identified ($k = 1$), whereas in the restructured surface (b), different layers are exposed ($k > 1$). Solid line indicates the crystal/vacuum interface; dashed lines indicates the layers forming the interface.

where p is the number of layers forming the restructured surface, and $n_{k,\sigma}$ and $F_{k,\sigma}$ are the surface density and free energy, respectively, of the atoms in the k-th layer of the face σ.

The free energy per atom, F, was determined by supposing that each atom coincides with a three-dimensional harmonic oscillator whose motion is not coupled to that of the other atoms.[13] In this treatment, F_b and $F_{k,\sigma}$ are as follows

$$F_b = \frac{\psi_b}{2} + \frac{1}{2}\sum_{j=1}^{3} h\nu_{j,b} + k_B T \ln \prod_{j=1}^{3}(1 - e^{-h\nu_{j,b}/k_B T}) \tag{A3}$$

$$F_{k,\sigma} = \frac{\psi_{k,\sigma}}{2} + \frac{1}{2}\sum_{j=1}^{3} h\nu_{k,j,\sigma} + k_B T \ln \prod_{j=1}^{3}(1 - e^{-h\nu_{k,j,\sigma}/k_B T}) \tag{A4}$$

where $\Psi/2$ is the potential energy per atom; $\upsilon_{j,b}$ and $\upsilon_{k,j,\sigma}$ are the vibrational frequencies along the axis j of the atom in the bulk and in the k-th layer of the surface σ, respectively; h and k_B are the Planck's and Boltzmann's constants, respectively. Equations A3 and A4 are valid for high temperatures ($k_B T \gg h\upsilon$). By inserting eqs A3 and A4 in eq A2, we obtain

$$\gamma_\sigma(T) = \sum_{k=1}^{p}\left[n_{k,\sigma}\left(\frac{\psi_{k,\sigma} - \psi_b}{2}\right)\right] + \sum_{k=1}^{p}\left\{\frac{n_{k,\sigma}}{2}\sum_{j=1}^{3}[h(\nu_{k,j,\sigma} - \nu_{j,b})]\right\} + k_B T \sum_{k=1}^{p}\left(n_{k,\sigma}\ln\prod_{j=1}^{3}\frac{1 - e^{-h\nu_{k,j,\sigma}/k_B T}}{1 - e^{-h\nu_{j,b}/k_B T}}\right) \tag{A5}$$

Equation A5 can be simplified (i) by considering $k_BT \gg h\nu$, (ii) substituting in the second term $\nu_{j,b} = k_B\theta/h$, where θ is the Debye temperature, and (iii) noting that $\gamma_\sigma(0) = \sum_{k=1}^{p} [n_{k,\sigma}(\psi_{k,\sigma} - \psi_b)/2]$ is the surface energy at 0 K. One then obtains

$$\gamma_\sigma(T) = \gamma_\sigma(0) + \frac{k_B\theta}{2}\sum_{k=1}^{p}\left[n_{k,\sigma}\sum_{j=1}^{3}\left(\frac{\nu_{k,j,\sigma}}{\nu_{j,b}} - 1\right)\right] + k_BT\sum_{k=1}^{p}\left(n_{k,\sigma}\ln\prod_{j=1}^{3}\frac{\nu_{k,j,\sigma}}{\nu_{j,b}}\right) \quad \text{(A6)}$$

It is evident from eq A6 that the surface energy undergoes a linear decrease with temperature, because the vibration frequencies for surface atoms are expected to be lower than those in the bulk.

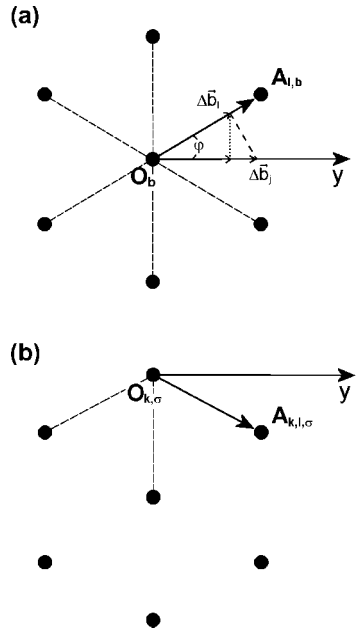

Figure A2. First neighbor polyhedron around the atom O_b in the (a) bulk and the (b) atom $O_{k,\sigma}$ on the surface.

Equation A6 can be further simplified by considering: (i) a crystal in which an atom O of mass M (Figure A2) vibrates inside a first neighbor polyhedron of m atoms, described by bond vectors $\vec{b}_l$ ($l = 1,..., m$) and (ii) the force acting on the atom O is described by the Hooke's law, $\vec{f}_l = -K\Delta\vec{b}_l$, where K is the force constant (harmonic isotropic oscillator) and $\Delta\vec{b}_l$ is the displacement along $\vec{b}_l$. Furthermore, instead of considering the displacement of the atom along the $\vec{b}_l$ vector, one can take a more general displacement of O in the cavity along the axis y, described by the unit vector $\vec{j}$. The displacement and the force acting along $\vec{b}_l$ can then be expressed as $\Delta\vec{b}_l = \Delta\vec{b}_j\cos\varphi$ and $\vec{f}_l = -K\Delta\vec{b}_j\cos\varphi$, respectively. The component of $\vec{f}_l$ on the axis $\vec{j}$, for the atom O_b in the bulk ($f_{l,j,b}$) and the atom $O_{k,\sigma}$ on the surface ($f_{k,l,j,\sigma}$), turns out to be

$$f_{l,j,b} = -K\Delta b_l\cos\varphi_{l,j,b} = -K\Delta b_j\cos^2\varphi_{l,j,b} \quad \text{(A7)}$$

$$f_{k,l,j,\sigma} = -K\Delta b_l\cos\varphi_{k,l,j,\sigma} = -K\Delta b_j\cos^2\varphi_{k,l,j,\sigma} \quad \text{(A8)}$$

where $\varphi_{k,l,j,\sigma}$ is the angle formed by the axis j and a vector $A_{k,l,\sigma} - O_{k,\sigma}$ joining an atom $O_{k,\sigma}$ in the k-th layer of the surface σ to an atom $A_{k,l,\sigma}$ of the first neighbor polyhedron centered on $O_{k,\sigma}$. Further, $\varphi_{l,j,b}$ is the angle formed by the axis j and a vector joining an atom O_b in the bulk and an atom $A_{l,b}$ of the first neighbor polyhedron centered on O_b. By considering all the m atoms (m_b and $m_{k,\sigma}$ for a polyhedron centered in the bulk and on the surface, respectively), the whole forces acting on the atom O in the bulk and on the surface σ are

$$f_{j,b} = \sum_{l=1}^{m_b} f_{l,j,b} = \sum_{l=1}^{m_b} -K\Delta b_j\cos^2\varphi_{l,j,b} = -K'\Delta b_j \quad \text{(A9)}$$

$$f_{k,j,\sigma} = \sum_{l=1}^{m_{k,\sigma}} f_{k,l,j,\sigma} = \sum_{l=1}^{m_{k,\sigma}} -K\Delta b_j\cos^2\varphi_{k,l,j,\sigma} = -K''\Delta b_j \quad \text{(A10)}$$

where $K' = \sum_{l=1}^{mb} K\cos^2\varphi_{l,j,b}$ and $K'' = \sum_{l=1}^{mk,\sigma} K\cos^2\varphi_{k,l,j,\sigma}$. Then, for bulk and surface, the frequency of an harmonic oscillator is given by

$$\nu_{j,b} = \frac{1}{2\pi}\sqrt{\frac{K'}{M}} \quad \text{(A11)}$$

$$\nu_{k,j,\sigma} = \frac{1}{2\pi}\sqrt{\frac{K''}{M}} \quad \text{(A12)}$$

From eqs A11 and A12, it results that

$$\frac{\nu_{k,j,\sigma}}{\nu_{j,b}} = \left(\frac{\sum_{l=1}^{m_{k,\sigma}}\cos^2\varphi_{k,l,j,\sigma}}{\sum_{l=1}^{m_b}\cos^2\varphi_{l,j,b}}\right)^{\frac{1}{2}} \quad \text{(A13)}$$

and by inserting eq A13 in eq A6, we finally obtain

$$\gamma_\sigma(T) = \gamma_\sigma(0) + \frac{k_B\theta}{2}\sum_{k=1}^{p}\left\{n_{k,\sigma}\sum_{j=1}^{3}\left[\left(\frac{\sum_{l=1}^{m_{k,\sigma}}(\cos\varphi_{k,l,j,\sigma})^2}{\sum_{l=1}^{m_b}(\cos\varphi_{l,j,b})^2}\right)^{\frac{1}{2}} - 1\right]\right\} + k_BT\sum_{k=1}^{p}\left[n_{k,\sigma}\ln\prod_{j=1}^{3}\left(\frac{\sum_{l=1}^{m_{k,\sigma}}(\cos\varphi_{k,l,j,\sigma})^2}{\sum_{l=1}^{m_b}(\cos\varphi_{l,j,b})^2}\right)^{\frac{1}{2}}\right] \quad \text{(A14)}$$

which is nothing else than eq 6 in the main text.

The Kern's model is a harmonic one; it was developed for a solid in which the phonon frequencies are independent of T and V (volume). In a real solid, the interactions between atoms are affected in different ways by changes of the thermodynamic conditions and therefore the phonon frequencies should be written as a function of T and V (anharmonic case). Moreover, in the Kern's model, only interactions between first neighbor atoms were considered, whereas a more detailed description of ionic crystals needs the consideration of long-range interactions.

Supporting Information Available: Tables listing the lattice parameters and atomic coordinates of the 20-layer (100) and 9-layer (111) slabs optimized at DFT level (PDF). This material is available free of charge via the Internet at http://pubs.acs.org.

References

(1) Walker, D.; Verma, P. K.; Cranswick, L. M. D.; Jones, R. L.; Clark, S. M.; Buhre, S. *Am. Mineral.* **2004**, *89*, 204–210.
(2) Knoppik, D.; Lösch, A. *J. Cryst. Growth* **1976**, *34*, 332–336. (a) Knoppik, D.; Bartscherer, H. Ch. *J. Cryst. Growth* **1976**, *36*, 342–344. (b) Heyraud, J. C.; Mètois, J. J. *J. Cryst. Growth* **1987**, *84*, 503–508.
(3) Shi, A. C.; Wortis, M. *Phys. Rev. B* **1988**, *37*, 7793–7805.
(4) Kern, R. *Bull. Soc. Fr. Miner. Cristallogr.* **1953**, *76*, 391. (b) Bienfait, M.; Boistelle, R.; Kern, R. Adsorption et Croissance Cristalline. In *Colloques Internationaux du Centre National de la Recherche Scientifique*; Kern, R., Ed.; CNRS: Paris, 1965; Vol. 152, pp 515−535.
(5) Radenović, N.; van Enckevort, W.; Verwer, P.; Vlieg, E. *Surf. Sci.* **2003**, *523*, 307–315. (a) Radenović, N.; van Enckevort, W.; Vlieg, E.

J. Cryst. Growth **2004**, *263*, 544–551. (b) Radenović, N.; van Enckevort, W.; Kaminski, D.; Heijna, M.; Vlieg, E. *Surf. Sci.* **2005**, *599*, 196–206.
(6) Johnsen, A. *Wachstum und Auflösung der Kristallen*; Engelmann: Leipzig, Germany, 1910.
(7) Rohr, F.; Wirth, K.; Libuda, J.; Cappus, D.; Bäumer, M.; Freund, H. J. *Surf. Sci.* **1994**, *315*, L977–L982. (a) Langell, M. A.; Berrie, C. L.; Nassir, M. H.; Wulser, K. W. *Surf. Sci.* **1994**, *320*, 25–38.
(8) Wander, A.; Bush, I. J.; Harrison, N. M. *Phys. Rev. B* **2003**, *68*, 233405.
(9) Lacmann, R., Adsorption et Croissance Cristalline. In *Colloques Internationaux du Centre National de la Recherche Scientifique*; Kern, R., Ed.; CNRS: Paris, 1965; Vol. 152, pp 195−214.
(10) Wolf, D. *Phys. Rev. Lett.* **1992**, *68*, 3315–3318.
(11) Ventrice, C. A.; Bertrams, Th.; Hannemann, H.; Brodde, A.; Neddermeyer, H. *Phys. Rev. B.* **1994**, *49*, 5773–5776. (a) Bertrams, Th.; Brodde, A.; Hannemann, H.; Ventrice, C. A.; Wilhelmi, G.; Neddermeyer, H. *Appl. Surf. Sci.* **1994**, *75*, 125–132. (b) Barbier, A.; Renaud, G.; Mocuta, C.; Stierle, A. *Surf. Sci.* **1999**, *433*−*435*, 761–764. (c) BarbierA.; Mocuta, C.; Kuhlenbeck, H.; Peters, K. F.; Richter, B.; Renaud, G. *Phys. Rev. Lett.* **2000**, *84*, 2897–2900.
(12) Massaro, F. R.; Pastero, L.; Rubbo, M.; Aquilano, D. *J. Cryst. Growth* **2008**, *310*, 706–715.
(13) Kern, R., The Equilibrium Form of Crystals. In *Morphology of Crystals*; Sunagawa, I., Ed.; Terra Scientific Publishing Company: Tokyo, 1987; Part A, pp. 77−203.
(14) Dovesi, R.; Saunders, V. R.; Roetti, C.; Orlando, R.; Zicovich-Wilson, C. M.; Pascale, F.; Civalleri, B.; Doll, K.; Harrison, N. M.; Bush, I. J.; D'Arco, Ph.; Llunell, M. *CRYSTAL06 User's Manual*; University of Torino; Torino, Italy, 2006.
(15) Pisani, C.; Dovesi, R.; Roetti, C. *Hartree-Fock Ab-Initio Treatment of Crystalline Systems, Lecture Notes in Chemistry*; Springer: New York, 1988.
(16) Becke, A. D. *J. Chem. Phys.* **1993**, *98*, 5648–5652.
(17) Becke, A. D. *Phys. Rev. A* **1988**, *38*, 3098–3100.
(18) Monkhrost, H. J.; Pack, J. D. *Phys. Rev. B* **1976**, *13*, 5188–5192.
(19) Dovesi, R.; Roetti, C.; Freyria Fava, C.; Prencipe, M.; Saunders, V. R. *Chem. Phys.* **1991**, *156*, 11–19.
(20) Aprà, E.; Causà, M.; Prencipe, M.; Dovesi, R.; Saunders, V. R. *J. Phys.: Condens. Matter* **1993**, *5*, 2969–2976.
(21) Civalleri, B.; D'Arco, Ph.; Orlando, R.; Saunders, V. R.; Dovesi, R. *Chem. Phys. Lett.* **2001**, *348*, 131–138.
(22) Dovesi, R.; Civalleri, B.; Orlando, R.; Roetti, C.; Saunders, V. R. Ab initio Quantum Simulation in Solid State Chemistry. In *Reviews in Computational Chemistry*; Lipkowitz, B. K., Larter, R., Cundari, T. R., Eds.; John Wiley & Sons Inc: New York, 2005; Vol. 21, pp 1−125.
(23) Prencipe, M.; Zupan, A.; Dovesi, R.; Aprà, E.; Saunders, V. R. *Phys. Rev. B* **1995**, *51*, 3391–3396.
(24) Vogt, J.; Weiss, H. *Surf. Sci.* **2001**, *491*, 155–168.
(25) Kashihara, Y.; Kimura, S.; Harada, J. *Surf. Sci.* **1989**, *214*, 477–492.
(26) Roberts, J. G.; Hoffer, S.; Van Hove, M. A.; Somorjai, G. A. *Surf. Sci.* **1999**, *437*, 75–85.
(27) Li, B.; Michaelides, A.; Scheffler, M. *Phys. Rev. B* **2007**, *76*, 075401.
(28) Mayer, J. E. *J. Chem. Phys.* **1933**, *1*, 270–279.
(29) Catlow, C. R. A.; Diller, K. M.; Norgett, M. J. *J. Phys. C* **1977**, *10*, 1395–1412.
(30) Perdew, J. P.; Zunger, A. *Phys. Rev. B* **1981**, *23*, 5048–5079.
(31) Perdew, J. P.; Burke, K.; Ernzerhof, M. *Phys. Rev. Lett.* **1996**, *77*, 3865–3868. (a) Perdew, J. P.; Burke, K.; Ernzerhof, M. *Phys. Rev. Lett.* **1997**, *78*, 1396.
(32) Wu, Z.; Cohen, R. E. *Phys. Rev. B* **2006**, *73*, 235116.
(33) Varshni, Y. P.; Konti, A. *J. Phys. C* **1972**, *5*, 2562–2566.
(34) *Handbook of Chemistry and Physics*, 80th ed.; Lide, D. R., Ed.; CRC Press: Boca Raton, FL, 1999.
(35) Zykova-Timan, T.; Ceresoli, D.; Tartaglino, U.; Tosatti, E. *Phys. Rev. Lett.* **2005**, *94*, 176105.
(36) Fumi, F. G.; Tosi, M. P. *J. Phys. Chem. Solids* **1964**, *25*, 31–43.
(37) Mulheran, P. A. *Modell. Simul. Mater. Sci. Eng.* **1994**, *2*, 1123–1129.
(38) Hunt, R. A.; Gale, B. *J. Phys. C* **1973**, *6*, 3571–3584.
(39) Radenović, N. The Role of Impurities on the Morphology of Nacl Crystals. An Atomic Scale View. Ph.D. Thesis, University of Nijmegen, Nijmegen, The Netherlands, 2006.

CG8000027